RSC Advances

PAPER

View Article Online
View Journal | View Issue

Cite this: *RSC Adv.*, 2019, **9**, 216

New ferrocenyl-containing organic hole-transporting materials for perovskite solar cells in regular (n-i-p) and inverted (p-i-n) architectures†

Jingwen Jia, Liangsheng Duan, Yu Chen, * Xueping Zong, Zhe Sun, Quanping Wu and Song Xue*

Received 29th October 2018
Accepted 8th December 2018

DOI: 10.1039/c8ra08946a

rsc.li/rsc-advances

Three triphenylamine derivatives containing ferrocenyl groups (**JW6**, **JW7** and **JW8**) were synthesized by facile syntheses. Their HOMO levels match the valence band energy of $CH_3NH_3PbI_3$. The introduction of ferrocenyl was aimed to obtain hole transporting materials with high mobility for perovskite solar cells. **JW7** shows higher hole mobility (4.2×10^{-4} cm^2 V^{-1} s^{-1}) than **JW6** (1.3×10^{-4} cm^2 V^{-1} s^{-1}) and **JW8** (1.5×10^{-4} cm^2 V^{-1} s^{-1}). Their film-forming properties are affected by their molecule structures. The methoxyl and *N*,*N*-dimethyl terminal substituents of **JW7** and **JW8** are beneficial for having better solubility than **JW6**. The regular mesoporous TiO_2-based perovskite solar cells (n-i-p) and the inverted planar heterojunction perovskite solar cells (p-i-n) fabricated using **JW7** show the highest power conversion efficiency of 9.36% and 11.43% under 100 mW cm^{-2} AM1.5G solar illumination. For p-i-n cells, the standard HTM PEDOT-based cell reaches an efficiency of 12.86% under the same conditions.

1 Introduction

Perovskite solar cells have attracted much attention due to the high photovoltaic performance of the organolead halide.[1–7] The organolead halide perovskite was used as the light absorber in liquid-based dye-sensitized solar cells (DSSCs), and showed a power conversion efficiency (PCE) of 3.8% in 2009. The initial PCE of the solid-state perovskite solar cells was 9.7% in 2012.[8,9] Recently, PCE of perovskite solar cells has been over 22%.[10] The commonly reported $CH_3NH_3PbI_3$ was used in the first solid-state PSC, and a solid hole-transport layer was made of 2,20,7,70-tetrakis-(*N*,*N*-di-*p*-methoxyphenylamine)-9,90-spirobifluorene (spiro-OMeTAD), which shows good charge extraction and improves the long-term stability of the device.[9,11–15] It is necessary to place the perovskite between an n-type semiconductor layer and a p-type semiconductor layer, according to the structure of traditional PSCs,[16] for charge separation and transport in a PSC device. Organic small-molecule HTMs such as spiro-OMeTAD are commonly used as p-type semiconductor materials for PSCs. Compared with inorganic HTMs and organic polymer HTMs, organic small-molecule HTMs have the advantages of facile synthesis, flexible modification of structure, and easy purification.[17–22] Organic small-molecule HTMs can reach high hole mobility by possessing tunable energy levels, suitable solubility in organic solvents, and good film-forming properties.[23–26]

Ferrocene is an organometallic compound with a sandwich structure. Ferrocene and its derivatives are widely used in electrochemical sensors, biomedicine, chemical catalysts and photovoltaic materials due to their good redox abilities.[27–30] Ferrocene can also act as a suitable electron-donating unit and can be easily functionalized, due to which it has been reacted with small molecules for conjugation. Ferrocene-containing triphenylamine derivatives have been reported because of their good light-harvesting ability and fast charge regeneration.[31,32] Ferrocenyl-substituted triphenylamines are used as sensitizers in DCCCs, and an inserted π-linker between ferrocene and triphenylamine is beneficial for charge transport in the molecule.[33–35] Structural changes have a significant influence on electron delocalization though the entire molecule. Ferrocenyl-substituted triphenylamines have also been used as p-type redox promoters in electrochromic display devices, and they can form a film layer by spin-coating.[36] Therefore, ferrocene is a promising candidate for photovoltaic materials. In our research, new ferrocenyl-substituted triphenylamine derivatives were synthesized, and they were used as organic small-molecule HTMs to construct PSCs. To the best of our knowledge, this is the first time that organic small molecules containing ferrocene have been reported in PSCs.

In this study, three new ferrocene-containing compounds (**JW6**, **JW7** and **JW8**) were prepared, and their structures are shown in Scheme 1. In **JW6**, **JW7** and **JW8** molecules, biferrocene groups were connected with triphenylamines *via* triple bonds, and a double bond was also introduced to link a moiety of triphenylamine, bis(4-methoxyphenyl)methane and 4,4′-methylenebis(*N*,*N*-

Tianjin Key Laboratory of Organic Solar Cells and Photochemical Conversion, School of Chemistry & Chemical Engineering, Tianjin University of Technology, Tianjin 300384, PR China. E-mail: cytjut@163.com; xuesong@ustc.edu.cn

† Electronic supplementary information (ESI) available. See DOI: 10.1039/c8ra08946a

dimethylaniline), which can adjust the solubility, energy levels and charge transport. Theoretical calculations were performed to observe the optimized geometric structures and frontier molecular orbitals of the three compounds. Spectral and electrochemical measurements were applied for the determination of light absorption and energy levels. Differential scanning calorimetry (DSC) was performed for analysing the thermal stability of **JW6**, **JW7** and **JW8**. PSCs based on **JW6**, **JW7** and **JW8** were fabricated, and we found that the concentration of HTM solution significantly influenced the device performance. In the inverted planar heterojunction perovskite solar cells (p-i-n), the concentration of HTMs was 5 mg mL^{-1} without any dopant. The PCE of p-i-n cells based on the studied HTMs reached 89% of the PCE of those cells based on the standard HTM (poly(3,4-ethylenedioxythiophene), PEDOT). In devices of the regular mesoporous TiO_2-based PSCs (n-i-p), different concentrations of HTM solutions were spin-coated by adding only 4-*tert*-butylpyridine (TBP). A low concentration of 10 mg mL^{-1} was good for the studied HTM to establish excellent contact with the perovskite layer. Among the three compounds, **JW7** showed better photovoltaic performances than **JW6** and **JW8**. The structure–efficiency relationship of these ferrocene-containing HTMs was discussed based on the measurements of *J–V* characterizations and steady-state and time-resolved photoluminescence (PL) spectra. The hole mobility of the new HTMs was measured by space-charge-limited-current (SCLC), and charge recombination was studied by electrochemical impedance spectroscopy (EIS). Through this research we hope to provide some experimental basis for designing new HTMs for PSCs.

2 Experimental

2.1 Materials

All the starting materials used in this study were purchased from J&K Chemical, Energy Chemical or Sigma-Aldrich and used without further purification, unless otherwise stated. *N*,*N*-Dimethylformamide (DMF) and tetrahydrofuran (THF) were dried using 200 mesh molecular sieve and sodium metal, respectively.

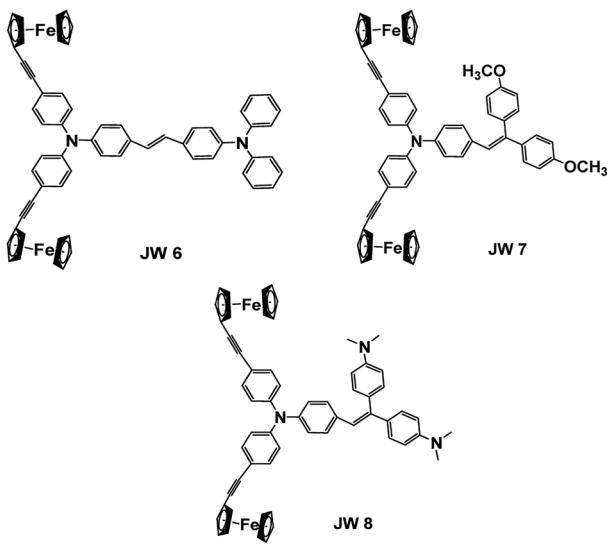

Scheme 1 Chemical structures of JW6, JW7 and JW8.

2.2 Fabrication of PSCs

In this study, two architectures of PSCs were fabricated. The conventional n-i-p type PSCs (FTO/TiO_2/perovskite/HTM/Ag) were fabricated according to the published method.[37] The main study was focussed on the inverted p-i-n type of PSCs (ITO/HTM/perovskite/PCBM/BCP/Ag). In brief, ITO glasses were successively washed using a special cleaner, acetone, water and ethanol, and then covered with HTM layer (5 mg mL^{-1}) by spinning at 4000 rpm for 40 s. This first layer was sintered at 100 °C for 10 min. By the sequential deposition method, a perovskite layer was covered on the HTM layer. After the perovskite precursor solution (461 mg PbI_2, 159 mg MAI, 70.9 μL DMSO and 634.92 μL DMF) was spin-coated at 5000 rpm for 25 s in a nitrogen filled glovebox, the device was annealed at 100 °C for 10 min. Then, PCBM (20 mg mL^{-1}) in CB and BCP (0.5 mg mL^{-1}) in isopropanol were spin-coated on the perovskite layer at 4000 rpm for 40 s. The PCBM layer was annealed at 80 °C for 10 min, while BCP was only spin-coated on the PCBM layer without any heating. Finally, Ag was vacuum-evaporated on the top of the device as the counter electrode.

2.3 Characterizations

^{1}H NMR and ^{13}C NMR spectra were recorded on a Bruker AM-400 spectrometer. The chemical shifts were reported against TMS. High resolution mass spectra were obtained on a Micromass GCT-TOF mass spectrometer. UV-vis absorption spectra were recorded on a SHIMADZU UV-2600 spectrophotometer. Photoluminescence (PL) measurements were recorded on a HITACHI F-4500 fluorescence spectrophotometer at 500 nm excitation wavelength. Cyclic voltammetry (CV) measurements were recorded using a Zennium electrochemical workstation (ZAHNER, Germany) under a three-electrode system, platinum was used as the working electrode, Ag/AgCl electrode was used as the reference electrode, and Pt-wires were used as the counter electrode. Electrochemical impedance spectroscopy (EIS) in the frequency range from 200 mHz to 100 kHz was performed with a Zennium electrochemical workstation (ZAHNER, Germany) in the dark with the alternate current amplitude set at 10 mV. Current–voltage (*J–V*) characteristics of PSCs were measured using a Keithley 2400 digital SourceMeter controlled by a computer under a standard AM 1.5 solar simulator (Oriel 91160-1000 (300 W) Solar Simulator). Incident photon-to-current conversion efficiency (IPCE) for PSCs was recorded on the QTest Station 2000 IPCE measurement system, CROWNTECH, USA. The space-charge-limited-current (SCLC) method was used to measure the hole mobility of HTMs using the equation:[37]

$$J = \frac{9}{8}\mu\varepsilon_0\varepsilon_r\frac{V^2}{d^3}$$

2.4 Synthesis of JW6, JW7 and JW8

The synthesis routes for **JW6**, **JW7** and **JW8** are shown in Scheme 2. The intermediates of compounds **1–7** have been reported in literature reports.[34,38–41]

General procedure for the synthesis of compounds JW6, JW7 and JW8. Compounds **7a–c** (0.677 mmol) were dissolved using anhydrous THF in a 100 mL two-neck round-bottom flask under N_2. After the temperature dropped to 0 °C, the THF solution of *t*-BuOK (0.880 mmol) was added dropwise, and the solution turned yellow. The reaction was kept at 0 °C for 1 hour. Then, THF solution of **4** (0.564 mmol) was added slowly. The mixture was then placed at room temperature and stirred overnight. Then, saturated NH_4Cl was added to stop the reaction and the product was extracted with dichloromethane. The combined organic layer was washed with brine and dried over anhydrous Na_2SO_4. The solvent was evaporated, and the remaining crude product was purified by column chromatography to obtain the desired compounds **JW6**, **JW7** and **JW8**.

Characterization details for the synthesis of **JW6**, **JW7** and **JW8** are provided in ESI.†

3 Results and discussion

3.1 Spectral, electrochemical and thermal stability measurements

Suitable HOMO and LUMO levels are important for HTMs to achieve hole transport in a PSC device. The HOMO levels matching the valence band energy of $CH_3NH_3PbI_3$ are suitable for fabricating efficient PSCs. In this study, the energy levels of the three HTMs were determined by spectroscopic and electrochemical measurements. As shown in Fig. 1(a), UV-visible absorptions of **JW6**, **JW7** and **JW8** were measured in film and in dichloromethane solution. The energy gap (E_{0-0}) values of **JW6**, **JW7** and **JW8** were calculated from the onset wavelengths of the absorption spectra in solution, which were 2.92 eV, 3.01 eV and 2.85 eV, respectively. **JW8** showed the smallest E_{0-0} value among the three HTMs, suggesting that **JW8** possesses larger π-conjugation than **JW6** and **JW7**. This was

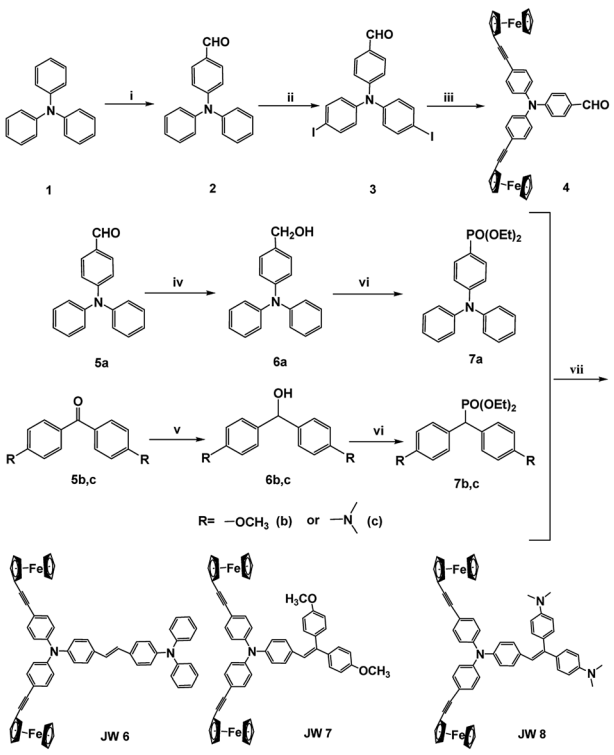

Scheme 2 The synthesis routes for **JW6**, **JW7** and **JW8**. Conditions: (i) $POCl_3$, DMF, 0 °C, 0.5 h then RT, 5 h; (ii) NIS, $CHCl_3$/AcOH(4 : 1), 100 °C, 0.5 h; (iii) ethynyl ferrocene, $Pd(PPh_3)_4$, Et_3N/THF (1 : 1), N_2, reflux, 6 h; (iv) $NaBH_4$, EtOH, NaOH, N_2, 0 °C, 0.5 h then RT, 4 h; (v) $NaBH_4$, i-PrOH, H_2O, N_2, reflux, 6 h; (vi) $P(OEt)_3$, I_2, RT, 5 h; (vii) 4, *t*-BuOK, THF, RT, 10 h.

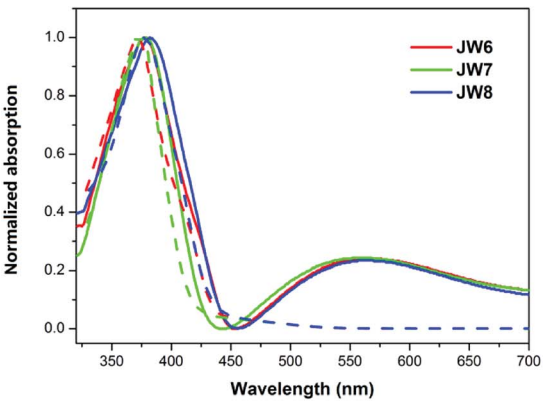

(a)

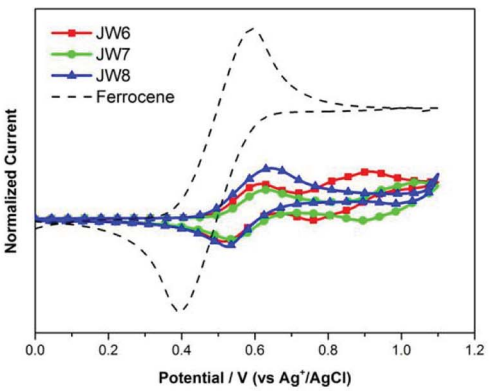

(b)

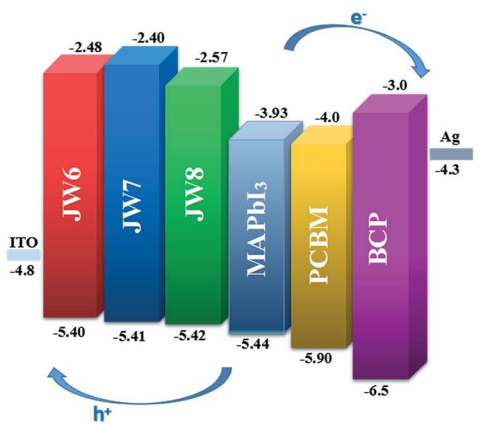

(c)

Fig. 1 (a) Absorption spectra of **JW6**, **JW7** and **JW8** in film (solid line) and dichloromethane solution (dash line); (b) cyclic voltammetry of **JW6**, **JW7** and **JW8**; (c) energy level scheme of **JW6**, **JW7** and **JW8** in a p-i-n type PSC.

Table 1 Spectral and electrochemical properties of JW6, JW7 and JW8

HTMs	λ_{max}^{sol} [a]/nm	λ_{max}^{film} [b]/nm	λ_{onset}/nm	Mobility/cm^2 V^{-1} s^{-1}	E_{0-0} [c]/eV	E_{HOMO} [d]/eV	E_{LUMO} [e]/eV
JW6	372	378	425	1.3×10^{-4}	2.92	−5.40	−2.48
JW7	372	378	412	4.3×10^{-4}	3.01	−5.41	−2.40
JW8	378	382	435	1.5×10^{-4}	2.85	−5.42	−2.57

[a] UV-vis spectra were measured in dichloromethane solution (5×10^{-6} M). [b] λ_{onset} is the onset wavelength of absorption spectrum. [c] Optical band gap was calculated from $1240/\lambda_{onset}$. [d] E_{HOMO} was calculated from the equation $E_{HOMO} = -4.7 - E_{ox}$. E_{ox} was standardized with ferrocene (0.63 V *vs.* NHE). [e] $E_{LUMO} = E_{HOMO} + E_{0-0}$.

consistent with the maximum absorption peak of **JW8** displaying a red shift in comparison with that of **JW6** and **JW7** both in dichloromethane solution and in solid-state film. The absorption of the studied HTMs bearing biferrocene was extended to around 450 nm. Cyclic voltammetry (CV) was used to measure the oxidation and reduction peaks of **JW6**, **JW7** and **JW8** in dichloromethane solution, and the CV curves are shown in Fig. 1(b). The HOMO levels of **JW6**, **JW7** and **JW8** were calculated from the equation $E_{HOMO} = -4.7 - E_{ox}$. The corresponding E_{HOMO} values of **JW6**, **JW7** and **JW8** were −5.40 eV, −5.41 eV and −5.42 eV, respectively. The E_{HOMO} values of the studied HTMs were very close and slightly higher than the valence band energy of $CH_3NH_3PbI_3$. Thus, it was easy for the new HTMs to accept holes transferred from $CH_3NH_3PbI_3$. The LUMO levels of **JW6**, **JW7** and **JW8** were calculated from the equation $E_{LUMO} = E_{HOMO} + E_{0-0}$, and the corresponding E_{LUMO} values were −2.48 eV, −2.40 eV and −2.57 eV, respectively. The higher E_{LUMO} value of **JW7** can more effectively prevent the electron transfer from $CH_3NH_3PbI_3$ to HTMs, and thus reduce charge recombination in the device. Moreover, the energy level scheme for a p-i-n cell is represented in Fig. 1(c), in which the difference in HOMO and LUMO energy levels of the three compounds can be clearly seen. The related spectral and electrochemical results are listed in Table 1.

Differential scanning calorimetry (DSC) was used to test the glass transition temperature (T_g) of **JW6**, **JW7** and **JW8**. DSC curves of these new HTMs are displayed in Fig. 2. **JW8** possessing 4,4′-methylenebis(*N*,*N*-dimethylaniline) and **JW7** possessing bis(4-methoxyphenyl)methane have higher T_g values (129 °C and 120 °C) than **JW6** possessing triphenylamine (116 °C). The DCS result shows **JW6**, **JW7** and **JW8** to have good stability in the amorphous state.

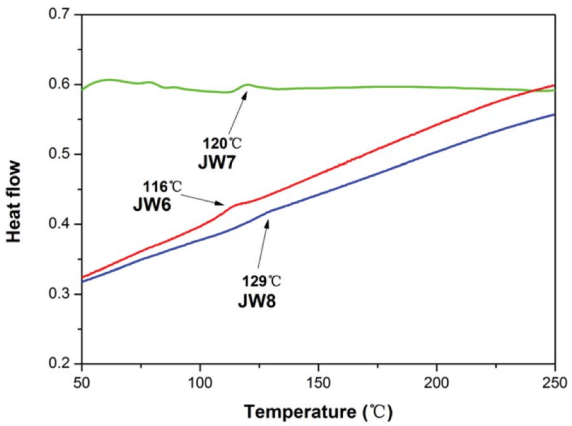

Fig. 2 DSC curves of **JW6**, **JW7** and **JW8**.

3.2 Theoretical calculations

The substituents have an important influence on the electron distribution and conjugated construction of HTM molecules. Theoretical calculations on the basis of DFT at the B3LYP/6-31G(g,d) level were used to optimize the geometric structures of the new HTMs. The optimized structures of **JW6**, **JW7** and **JW8** are given in Fig. S1,† and the representative bond lengths and dihedral angles are listed in Table S1 (seen in ESI†). The frontier molecular orbitals of the three compounds are shown in Fig. 3. The highest occupied molecular orbitals (HOMO) of the three compounds are almost delocalized over the whole molecule. The lowest unoccupied molecular orbitals (LUMO) are localized in the double bond part. The LUMO of **JW7** is transferred from the triphenylamine part to the (4-methoxyphenyl)methane section. As shown in Table S1,† the C–C bond lengths of ferrocenylethynyl and triphenylamine in the three compounds are the same (1.423 Å), and the C–N bond lengths of this triphenylamine are similar, which are 1.419 Å, 1.418 Å and 1.416 Å for **JW6**, **JW7** and **JW8**, respectively. **JW7** and **JW8** have a shorter C–N bond length, suggesting a longer π-conjugated

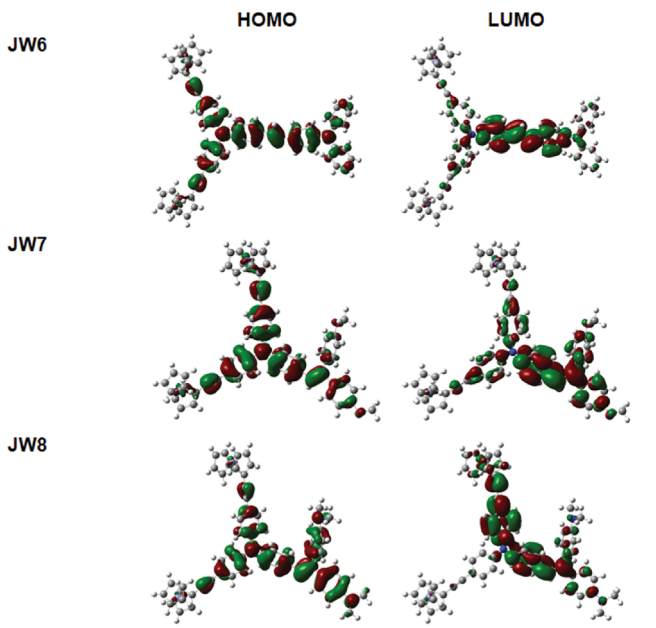

Fig. 3 Frontier molecular orbitals of **JW6**, **JW7** and **JW8**.

length. Moreover, **JW7** and **JW8** have similar C=C bond lengths of 1.468 Å and 1.467 Å, respectively. The C–C bonds of double bond and diphenylmethane group for **JW7** and **JW8** are 1.491 Å and 1.489 Å, respectively. Overall, **JW8** has the shortest bond length among the three HTMs. The dihedral angles of the two phenyl rings of the triphenylamine connecting ferrocenylethynyl in **JW6**, **JW7** and **JW8** are 40.9°, 39.4° and 37.9°, respectively. The dihedral angles between the double bond and the phenyl ring of diphenylmethane group in **JW7** and **JW8** are −26.9° and −25.2°, respectively. The data of dihedral angles also indicate that **JW7** and **JW8** have a more planar conjugated plane than **JW6**. Therefore, the results suggest that **JW7** and **JW8** may have a trend for faster charge transport than **JW6**. The device performances of the three compounds will be discussed in detail in Section 3.3.

3.3 Device performance

HTM solutions were prepared to be spin-coated for fabricating PSC devices, and two architectures of PSCs were constructed to evaluate the photovoltaic performances of the new HTMs-based cells. In the inverted planar heterojunction perovskite solar cells (p-i-n), the studied HTMs are used without any additives. The concentration of HTM solutions was 5 mg mL^{-1}. The p-i-n cells were based on the structure of ITO/HTM/perovskite/PCBM/BCP/Ag. Fig. 4 shows a cross-section SEM image of the p-i-n-type cell. The structure of the device is dense and neat. The fill factor (FF) of p-i-n cells fabricated by using **JW6**, **JW7** and **JW8** is higher than that of their n-i-p cells. The PCE of p-i-n cells based on **JW6**, **JW7** and **JW8** are 10.23%, 11.43% and 10.42%, respectively. The PCE of PSCs fabricated using the standard PEDOT is 12.86%. The corresponding *J–V* curves of p-i-n cells are shown in Fig. 5(a). In addition, device performances of p-i-n cells display replicability and stability. The photovoltaic parameters of eight cells of p-i-n-type PSCs fabricated using **JW7** are presented in Table S2.† They are kept at room temperature (25 °C) and in ambient air of 30% RH without encapsulation. Hysteresis test for p-i-n type PSCs based on the new HTMs was conducted, and the results are summarized in Table S3.† Fig. S2† exhibits the *J–V* plots of p-i-n type PSCs based on **JW7**

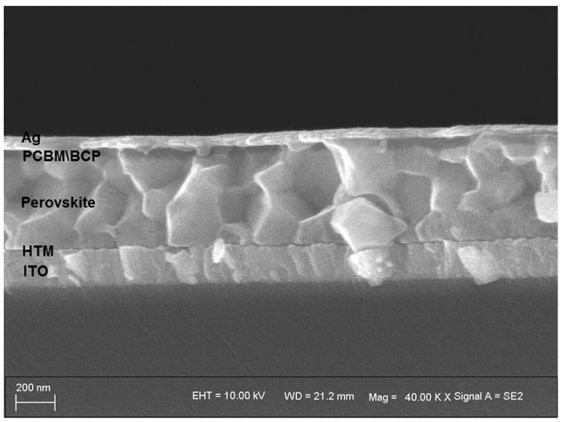

Fig. 4 Cross-section SEM image of the p-i-n type cell fabricated using JW7.

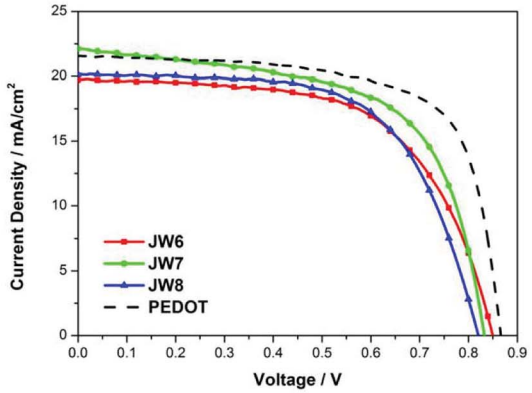

(a)

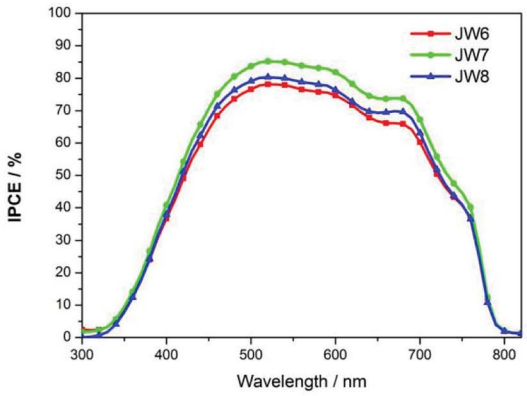

(b)

Fig. 5 (a) *J–V* characteristic curves and (b) IPCE spectra for p-i-n PSCs.

through reverse and forward bias at a scan rate of 0.1 V s^{-1}. The data of hysteresis test for p-i-n type PSCs fabricated using the standard PEDOT are also provided in Table S3† as a reference.

Results of the incident photon-to-current conversion efficiency (IPCE) spectra of p-i-n cells fabricated using **JW6**, **JW7** and **JW8** are shown in Fig. 5(b). The three HTMs have a wide range from 450 nm to 700 nm. The difference in J_{SC} is in accordance with that in the measured values in the order of **JW7** > **JW8** > **JW6** (Table 2).

Furthermore, data based on the space-charge-limited-current (SCLC) method was used to study the hole mobility of **JW6**, **JW7** and **JW8**. Fig. 6(a) shows the fitting current density–voltage (*J–V*) curves. The calculated values of the hole mobility of **JW6**, **JW7** and **JW8** were 1.3×10^{-4} cm^2 V^{-1} s^{-1}, 4.2×10^{-4} cm^2 V^{-1} s^{-1} and 1.5×10^{-4} cm^2 V^{-1} s^{-1}. **JW7** showed higher hole mobility than **JW6** and **JW8**, indicating that different substitutes

Table 2 *J–V* parameters of PSCs (p-i-n type) with JW6, JW7 and JW8

HTMs	V_{OC}/mV	J_{SC}/mA cm^{-2}	FF	PCE/%
JW6	850	19.73	0.61	10.23
JW7	833	22.13	0.62	11.43
JW8	820	20.17	0.63	10.42
PEDOT	867	22.26	0.69	12.86

had significant influence on the intermolecular charge transport of the studied HTMs. Photoluminescence (PL) measurements were recorded to study the charge extraction capability of **JW6**, **JW7** and **JW8**, and those for PEDOT were also recorded as a standard. Fig. 6(b) displays the steady-state PL spectra of the $CH_3NH_3PbI_3$ perovskite films without or with capping different HTMs. The PL band of the perovskite film is observed to be centered at 756 nm by excitation at 500 nm. All the bilayers show a drastic quenching of PL with respect to the pristine perovskite, following the order of perovskite/**JW7** > perovskite/**JW8** > perovskite/**JW6**. This suggests that **JW7** has a more positive effect on device performances than **JW6** and **JW8**, benefiting from the higher hole mobility and hole extraction capability.[42] Electrochemical impedance spectroscopy (EIS) was performed to further understand charge recombination in PSCs fabricated using **JW6**, **JW7** and **JW8**. Fig. 6(c) displays the Nyquist plots. The recombination resistance (R_{rec}) is represented by the large arc at low frequency. The R_{rec} value increases in the sequence of **JW8**, **JW7** and **JW6**, indicating that the device performances based on **JW8** are affected by faster charge recombination. Larger R_{rec} of **JW6** and **JW7** are beneficial for reducing charge recombination.[37] However, the device performances based on **JW6** are limited by relatively lower hole mobility, according to data of PL measurements. Therefore, **JW7** with the 4,4′-methylenebis(*N*,*N*-dimethylaniline) substituent shows a good performance in the inverted planar heterojunction perovskite solar cells.

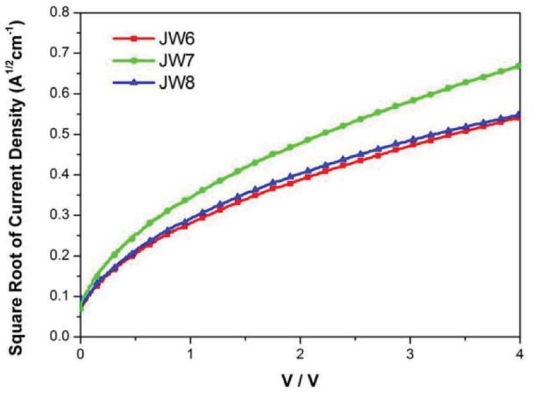

(a)

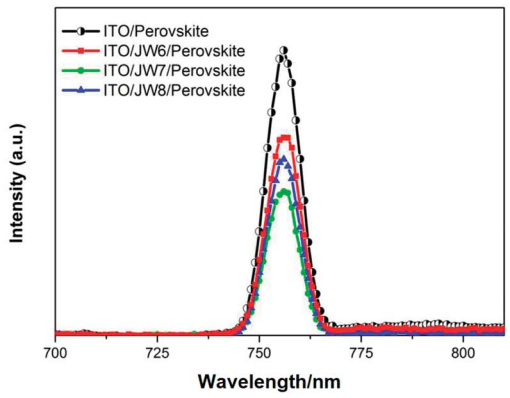

(b)

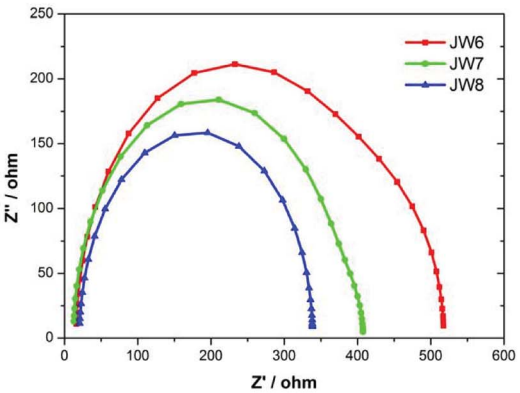

(c)

Fig. 6 (a) The space-charge-limited-current (SCLC) measurements of hole-only devices of ITO/HTM/PCBM/BCP/Ag based on **JW6**, **JW7** and **JW8**. (b) Steady-state and time-resolved photoluminescence (PL) spectra of **JW6**, **JW7** and **JW8**. (c) EIS for PSCs based on **JW6**, **JW7** and **JW8** measured in the dark under 0.9 V bias displayed in the form of Nyquist plots.

Table 3 *J*–*V* parameters of n-i-p type PSCs with different concentrations of **JW7**

Conditions	V_{OC}/mV	J_{SC}/mA cm^{-2}	FF	PCE/%
1[a]	825	9.64	0.28	2.23
2[a]	881	8.87	0.26	2.03
3[b]	865	19.24	0.52	8.65
4[b]	836	20.92	0.47	8.22
5[b]	870	18.99	0.47	7.77
6[b]	864	18.95	0.46	7.53
7[c]	842	19.50	0.57	9.36
8[c]	825	19.21	0.56	8.88
9[c]	847	18.45	0.53	8.28

[a] PSC covered with 30 mg mL^{-1} HTM. [b] PSC covered with 20 mg mL^{-1} HTM. [c] PSC covered with 10 mg mL^{-1} HTM.

In addition, different concentrations of **JW7** were tested in the regular mesoporous TiO_2-based perovskite solar cells (n-i-p). The structure of the n-i-p-type cells is FTO/TiO_2/perovskite/HTM/Ag. The photovoltaic parameters of the representative devices based on n-i-p-type PSCs are listed in Table 3. All the n-i-p cells are based on HTM solutions prepared by adding only TBP and without adding expensive additives such as LiTFSI.

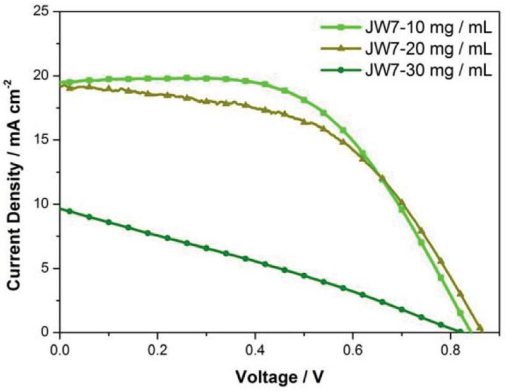

Fig. 7 *J*–*V* characteristic curves for PSCs (n-i-p type).

Fig. 7 shows the effect of different concentrations on n-i-p device performances determined by *J–V* measurements. When using **JW7** of 30 mg mL^{-1}, the value of photocurrent (J_{SC}) drops sharply, and the highest PCE is only 2.23%. The PCE increases to 8.65% when the concentration of **JW7** is reduced to 20 mg mL^{-1}. Furthermore, the device performances get even better when the concentration of HTM solution decreases to 10 mg mL^{-1}, and the PCE can reach 9.36%.

4 Conclusions

In this study, three triphenylamine derivatives containing ferrocene were synthesized and used as organic HTMs for fabricating efficient PSCs. The substitutes on their structures are different, which are triphenylamine for **JW6**, bis(4-methoxyphenyl)methane for **JW7** and 4,4′-methylenebis(*N*,*N*-dimethylaniline) for **JW8**. The maximum absorption wavelengths of the three compounds are around 370–380 nm and that of **JW8** (378 nm) has a red shift when compared with **JW6** (372 nm) and **JW7** (372 nm). Theoretical calculations show that **JW7** and **JW8** have a more planar conjugated structure. The three HTMs display T_g values beyond 110 °C. SCLC results show that **JW7** exhibits the highest hole mobility among the studied HTMs. In the inverted p-i-n-type of PSCs (ITO/HTM/perovskite/PCBM/BCP/Ag), **JW7** shows better photovoltaic performance than **JW6** and **JW8** under the same conditions, leading to a PCE of 11.43% (standard PEDOT, 12.86%). In the conventional n-i-p device of FTO/TiO_2/perovskite/HTM/Ag, the optimal concentration of HTM is 10 mg mL^{-1}. The corresponding highest PCE for these n-i-p cells was 9.36%, which were fabricated using **JW7** and adding TBP as the dopant. Therefore, ferrocene-containing materials have a great potential in perovskite solar cells, and there is a lot of work to be done in the development of these ferrocene-based HTMs for fabricating high-efficiency PSCs.

Conflicts of interest

There are no conflicts to declare.

Acknowledgements

This study was supported by the National Natural Science Foundation of China (21506164, 21671148, and 21576215).

Notes and references

1 N. Arora, M. Ibrahim Dar, A. Hinderhofer, N. Pellet, F. Schreiber, S. M. Zakeeruddin and M. Grätzel, *Science*, 2017, **358**, 768–771.
2 H. J. Snaith, *Nat. Mater.*, 2018, **17**, 372–376.
3 K. Mahmood, S. Sarwar and M. T. Mehran, *RSC Adv.*, 2017, **7**, 17044–17062.
4 T. Salim, S. Sun, Y. Abe, A. Krishna, A. C. Grimsdalea and Y. M. Lam, *J. Mater. Chem. A*, 2015, **3**, 8943–8969.
5 S. Wang, W. Yuan and Y. S. Meng, *ACS Appl. Mater. Interfaces*, 2015, **7**, 24791–24798.
6 F. Yang, D.-W. Kang and Y. –S. Kim, *RSC Adv.*, 2017, **7**, 19030–19038.
7 A. Yusoff, P. Gao and M. K. Nazeeruddin, *Coord. Chem. Rev.*, 2018, **373**, 258–294.
8 A. Kojima, K. Teshima, Y. Shirai and T. Miyasaka, *J. Am. Chem. Soc.*, 2009, **131**, 6050–6051.
9 H. Kim, C. Lee, J. Im, K. Lee, T. Moehl, A. Marchioro, S. Moon, R. Humphry-Baker, J. Yum, J. E. Moser, M. Grätzel and N. Park, *Sci. Rep.*, 2012, **2**, 591.
10 W. Yang, J. H. Noh, N. J. Jeon, Y. C. Kim, S. I. Ryu, J. Seo and S. Seok, *Science*, 2015, **348**, 1234–1237.
11 F. Santiago, J. Bisquert, L. Cevey, P. Chen, M. Wang, S. M. Zakeeruddin and M. Grätzel, *J. Am. Chem. Soc.*, 2009, **131**, 558–562.
12 N. J. Jeon, H. G. Lee, Y. C. Kim, J. Seo, J. H. Noh, J. Lee and S. Seok, *J. Am. Chem. Soc.*, 2014, **136**, 7837–7840.
13 C. S. Ponseca, E. M. Hutter, P. Piatkowski, B. Cohen, T. Pascher, A. Douhal, A. Yartsev, V. Sundström and T. J. Savenije, *J. Am. Chem. Soc.*, 2015, **137**, 16043–16048.
14 M. Jung, S. R. Raga, L. K. Ono and Y. Qi, *Sci. Rep.*, 2015, **5**, 9863.
15 A. Marchioro, J. Teuscher, D. Friedrich, M. Kunst and R. Krol, *Nat. Photonics*, 2014, **8**, 250–255.
16 X. Zhao and M. Wang, *Materials Today Energy*, 2018, **7**, 208–220.
17 Y. Wang, T. Su, H. Tsai, T. Wei and Y. Chi, *Sci. Rep.*, 2017, **7**, 7859.
18 F. Zhang, S. Wang, H. Zhu, X. Liu, H. Liu, X. Li, Y. Xiao, S. M. Zakeeruddin and M. Grätzel, *ACS Energy Lett.*, 2018, **3**, 1145–1152.
19 Y. Wu, Z. Wang, M. Liang, H. Cheng, M. Li, L. Liu, B. Wang and J. Wu, *ACS Appl. Mater. Interfaces*, 2018, **10**, 17883–17895.
20 K. Rakstys, A. Abate, M. I. Dar, P. Gao, V. Jankauskas, G. Jacopin, E. Kamarauskas, S. Kazim, S. Ahmad, M. Grätzel and M. K. Nazeeruddin, *J. Am. Chem. Soc.*, 2015, **137**, 16172–16178.
21 R. Grisorio, B. Roose, S. Colella, A. Listorti, G. P. Suranna and A. Abate, *ACS Energy Lett.*, 2017, **2**, 1029–1034.
22 M. S. Kang, S. D. Sung, I. T. Choi, H. Kim, M. Hong, J. Kim, W. Lee and H. K. Kim, *ACS Appl. Mater. Interfaces*, 2015, **7**, 22213–22217.
23 N. J. Jeon, H. Na, E. H. Jung, T. Y. Yang, Y. G. Lee, G. Kim, H. Shin, S. Seok, J. Lee and J. Seo, *Nat. Energy*, 2018, **3**, 682–689.
24 N. J. Jeon, J. Lee, J. H. Noh, M. K. Nazeeruddin and M. Grätzel, *J. Am. Chem. Soc.*, 2013, **135**, 19087–19090.
25 H. Nishimura, N. Ishida, A. Shimazaki, A. Wakamiya, A. Saeki, L. T. Scott and Y. Murata, *J. Am. Chem. Soc.*, 2015, **137**, 15656–15659.
26 W. Ke, P. Priyanka, S. Vegiraju, C. C. Stoumpos, I. Spanopoulos, C. Soe, T. J. Marks, M. C. Chen and M. G. Kanatzidis, *J. Am. Chem. Soc.*, 2018, **140**, 388–393.
27 A. Ghosh, S. Mishra, S. Giri, S. M. Mobin, A. Bera and S. Chatterjee, *Organometallics*, 2018, **37**, 1999–2002.

28 R. J. Durand, S. Achelle, S. Gauthier, N. Cabon, M. Ducamp, S. Kahlal, J. Saillard, A. Barsella and F. R. Guen, *Dyes Pigm.*, 2018, **155**, 68–74.
29 N. Dwadnia, J. Roger, N. Pirio, H. Cattey and J. C. Hierso, *Coord. Chem. Rev.*, 2018, **355**, 74–100.
30 J. C. Spiteri, A. D. Johnson, S. A. Denisov, G. Jonusauskas, N. D. McClenaghan and D. C. Magri, *Dyes Pigm.*, 2018, **157**, 278–283.
31 C. Su, Y. Ye, L. Xu and C. Zhang, *J. Mater. Chem.*, 2012, **22**, 22658–22662.
32 R. Maragani and R. Misra, *Tetrahedron*, 2014, **70**, 3390–3399.
33 R. Maragani, R. Misra, M. S. Roy, M. K. Singh and G. D. Sharma, *Phys. Chem. Chem. Phys.*, 2017, **19**, 8925–8933.
34 R. Misra, R. Maragani, K. R. Patel and G. D. Sharma, *RSC Adv.*, 2014, **4**, 34904–34911.
35 A. M. El-Zohry, J. Cong, M. Karlsson, L. Kloo and B. Zietz, *Dyes Pigm.*, 2016, **132**, 360–368.
36 C. H. Noh, S. H. Cho, K. Y. Song, T. R. Choi and T. Byk, *US pat.* 20080186564, 2008-08-07.
37 J. Zhang, B. Xu, L. Yang, C. Ruan, L. Wang, P. Liu, W. Zhang, N. Vlachopoulos, L. Kloo, G. Boschloo, L. Sun, A. Hagfeldt and E. Johansson, *Adv. Energy Mater.*, 2018, **8**, 1701209.
38 H. J. Snaith and M. Grätzel, *Appl. Phys. Lett.*, 2006, **89**, 262114.
39 W. Zhang, P. Liu, A. Sadollahkhani, Y. Li, B. Zhang, F. Zhang, M. Safdari, Y. Hao, Y. Hua and L. Kloo, *ACS Omega*, 2017, **2**, 9231–9240.
40 H. Shang, H. Fan, Q. Shi, S. Li, Y. Li and X. Zhan, *Sol. Energy Mater. Sol. Cells*, 2010, **94**, 457–464.
41 L. Zhang, Y. Liu, Z. Wang, M. Liang, Z. Sun and S. Xue, *Tetrahedron*, 2010, **66**, 3318–3325.
42 C. Huang, W. Fu, C. Li, Z. Zhang, W. Qiu, M. Shi, P. Heremans, A. Jen and H. Chen, *J. Am. Chem. Soc.*, 2016, **138**, 2528–2531.